Characteristic and Magnetic Field Analysis of a Non-magnetic Secondary Linear Induction Maglev Motor

Qin Wei, Fan Yu and LI SHUO
School of Electrical Engineering, Beijing Jiao-tong University, Beijing, China
09117341@bjtu.edu.cn. , *yfani@bjtu.edu.cn* , *10117333@bjtu.edu.cn* ,

ABSTRACT: The non-magnetic Secondary linear induction Maglev motor, which is Electro-dynamic System, is presented in this paper. The thrust and the levitation force of the proposed motor can be achieved simultaneously by using time varying magnetic fields, which create by 3-phase alternating current in primary winds, induct eddy field in secondary. This paper establishes a simplified two-dimensional model, studies the dynamic characteristic of the maglev, and gets lift and thrust force analytical solution. Finally, the thrust and normal force are measured to confirm the theoretical analysis. The experiment results show that the thrust and normal force which are computed are close to these which are measured.

1 INTRODUCTION

Maglev offer many attractive particular properties. 1) It is the only high-speed ground transportation system that can operate to speeds of 500 km/h. 2) It has lower power consumption, less noise, more safety and more comfort due to the absence of mechanical contact. 3) It has higher rates of acceleration and deceleration and a better climbing capability [1]-[2].

High-speed maglev ground transportation vehicles typically use either electromagnetic suspension (EMS) or electro-dynamic suspension (EDS) methods. EDS enables a large gap and stable running with no control, therefore it will be an important development direction of the maglev.

Nowadays the permanent magnets (PMs) EDS have been studied by many researchers such as Jonathan Bird and Thomas A. Lipo. However, the rapid translational motion of magnetic fields past conductors creates an unavoidable magnetic drag force, which tends to have rather a low levitation/ drag ratio. This paper has been focused on an innovative transportation system Non-magnetic Secondary Linear Induction Maglev Motor (NSLIM), this system uses time varying magnetic fields generate lift force, and the thrust force can be generated simultaneously [7].

It is well known that the accurate calculation of the field distribution is essential for the design of NSLIM machines. With the availability of powerful software tools, numerical analysis of the field distribution has become common practice. However, while numerical techniques, such as FEA analysis, provide an accurate means of determining the field distribution, they remain time-consuming. Therefore, by using 2-D electromagnetic model based on analytical solutions, magnetic fields of NSLIM machines shown in Fig.1 are computed. A finite element method simulation is performed to validate results obtained by the proposed method [3]-[4].

2 MACHINE CONSTRUCTION AND MODELING ANALYSIS

2.1 Machine construction

The Non-magnetic Secondary Linear Induction Maglev Motor prototype is shown in Fig. 1. The machine is constructed of the secondary and the primary, as shown in Fig. 2. 3-phase windings are placed in the slotted stator core to produce the time varying magnetic field and the nonmagnetic conducting secondary are mounted on the non-translate shaft。

The NSLIM offers some advantages over the conventional linear motor. It is considered due to the fact that lift force, and the thrust force can be generated simultaneously by NSLIM. The repulsive force is sufficiently large to suggest the possibility of its being used for suspending a high-speed train. On the other hand, the NSLIM also

offers a lower cost besides it is easy to manufacture.

The machine runs in a reciprocating linear motion, which runs forward and then moves backward after it reaches the end of the motion. A long-translator machine is the type selected for better overall performance.

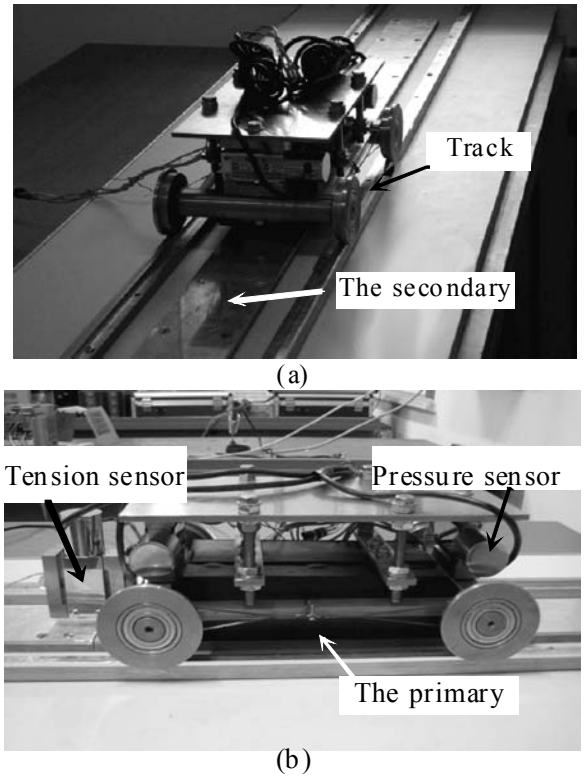

Figure1.NSLIM prototype

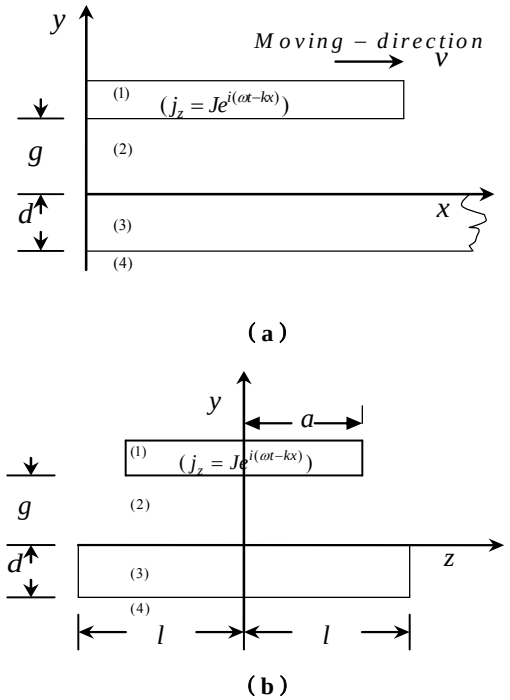

Figure2. 2D-model of the motor

Tab. 1 NSLIM SPECIFICATION

Parameter	Value	Parameter	Value
current frequency /Hz	30-100	air gap/mm	5-30
The secondary Conductivity/A	3.43e107	the number of slot z	12
the number of pole pairs	4	slot width b11/mm	8
The Diameter Of winding/mm	1.115	teeth width /mm	8
relative permeability of shaft material	1	stroke /mm	25.7
The primary width /m	0.01	Secondary width /m	0.15
The secondary height /mm	8-15	Max current/A	9
τ/mm	42	permeability of core material ,core	Infinity

2.2 NSLIM modeling and analysis

The 2D cross-section of the upper half of the machine is shown in Fig.2. A conducting plate of thickness d and the primary as Figure 2 divides space into four regions: region 1 the primary itself, region 2 (above the conducting plate and below the primary) is the air-gap I, region3 the conducting plate itself, and region4 (below the plate) is the air-gap II contains no magnetic sources or conducting material.

The geometry used to model the motor fields is shown in Figure2.Let the upper surface of the conducting plate coincide with the x -y plane (y = 0); the primary, which is located in a plane parallel to the surface of the conducting plate, at y =g + h, moves in the x direction.

To complete the problem definition and to get to a unique solution, the following boundary conditions are fixed: First, the primary windings are modeled as two imaginary sets of distributed phase windings laid on the primary iron surface, the traveling wave excitation surface currents k_s at the primary. In the flux linkage calculation, the slots effect is usually incorporated by applying the Carter coefficient. Second, the machine is assumed to be infinitively long and has a periodic construction. Third, the permeability of the stator core is assumed to be infinite whereas the relative permeability of the winding, air gap and permanent magnet as well as the shaft is assumed to be one [5]-[6].

Maxwell's and Poisson's equations for zone 3 are, respectively, given as:

$$\nabla \times B = \mu_0 J \quad \textbf{(1)}$$

$$\nabla \times E = -\frac{\partial B}{\partial t} \quad \textbf{(2)}$$

$$J = \sigma(E + v \times B) \quad \textbf{(3)}$$

Solving (1), (2) and (3), (1) can be written as:

$$\frac{\partial^2 B}{\partial x^2}+\frac{\partial^2 B}{\partial y^2}=i\mu_0 s\sigma\omega B=R^2 B \quad (4)$$

Where: $s=(v_s-v)/v_s$, $v_s=2p\tau$, τ **is the pole pitch;** v **is the velocity of the primary;** p **is the number of pole pairs;** $R^2=i\mu_0\sigma dv$; $\mu_0=4\pi\times10^{-7}$.

The equation (4), is satisfied when

$$B_x=b_x(y)e^{i(\omega t-kx)}$$

The derivations can be presented concisely:

$$B_{x3}=(A_1 ch\beta y+A_2 sh\beta y)e^{i(\omega t-kx)} \quad (5)$$

$$B_{y3}=(A_3 ch\beta y+A_4 sh\beta y)e^{i(\omega t-kx)} \quad (6)$$

Where: $k=\pi/\tau$; $\beta^2=k^2+R^2$

In the zone 2, can be written as:

$$\frac{\partial B_x}{\partial x}+\frac{\partial B_y}{\partial y}=0$$

The derivations can be presented concisely:

$$-ikA_1+\beta A_4=0 \quad (7)$$

$$-ikA_2+\beta A_3=0 \quad (8)$$

Maxwell's and Poisson's equations for zone 3 are, respectively, given as

$$B_{x2}=(A_5 ch\beta_1 y+A_6 sh\beta_1 y)e^{i(\omega t-kx)} \quad (9)$$

$$B_{y2}=(A_7 ch\beta_1 y+A_8 sh\beta_1 y)e^{i(\omega t-kx)} \quad (10)$$

where: $\beta_1=k$

In the zone 2, $\frac{\partial B_x}{\partial x}+\frac{\partial B_y}{\partial y}=0$ **, The derivations can be presented concisely**

$$-ikA_5+\beta_1 A_8=0 \quad (11)$$

$$-ikA_6+\beta_1 A_7=0 \quad (12)$$

In the zone 4, B is zeros when $y\to-\infty$ **, we can derivate the flux density as follows:**

$$B_{x4}=A_9 e^{ky}e^{i(\omega t-kx)} \quad (13)$$

$$B_{y4}=A_{10}e^{ky}e^{i(\omega t-kx)} \quad (14)$$

$$-ikA_9+\beta_1 A_{10}=0 \quad (15)$$

Boundary conditions are selected to solve the simultaneous field equations, as shown in (16), (17), (18), (19) and（20）:

$$A_1=A_5 \quad (16)$$

$$A_3=A_7 \quad (17)$$

$$A_1 ch(-\beta d)+A_2 sh(-\beta d)=A_9 e^{-kd} \quad (18)$$

$$A_3 ch(-\beta d)+A_4 sh(-\beta d)=A_{10}e^{-kd} \quad (19)$$

$$(A_5 chkg+A_6 shkg)=\mu_0 J_z \quad (20)$$

Solving （7）,（8）,（10）,（11）,（15）,（16）,（17）,（18）, （19）and （20）, The derivations can be presented concisely:

$$A_1=A_5=-\frac{i\beta}{k}\frac{\mu_0 J_z(kch\beta d+\beta sh\beta d)}{\Delta}$$

$$A_2=-\frac{i\beta}{k}\frac{\mu_0 J_z(\beta ch\beta d+ksh\beta d)}{\Delta}$$

$$A_3=A_7=\frac{\mu_0 J_z(\beta ch\beta d+ksh\beta d)}{\Delta}$$

$$A_4=\frac{\mu_0 J_z(kch\beta d+\beta sh\beta d)}{\Delta}$$

$$A_6=-iA_7=-i\frac{\mu_0 J_z(\beta ch\beta d+ksh\beta d)}{\Delta}$$

$$A_8=iA_5=\frac{\beta}{k}\frac{\mu_0 J_z(kch\beta d+\beta sh\beta d)}{\Delta}$$

$$F_{thrust}=\frac{L}{2\mu_0}\int_0^{\tau}\mathrm{Re}(B_{x3}\cdot B_{y3}^*)dx$$

$$F_{thrust}=\frac{L}{4\mu_0}\int_0^{\tau}\mathrm{Re}(B_{y3}\cdot B_{y3}^*-B_{x3}\cdot B_{x3}^*)dx$$

Where:

$\Delta=chkg(ksh\beta d+\beta ch\beta d)+shkg(\beta sh\beta d+kch\beta d)$, $\omega=2\pi f$, f **is the primary current frequency,** L **is the width of the motor.**

3 RESULTS AND DISCUSSION

In this section, the computer-simulation model constructed by the finite-element method (FEM) has been developed for software ANSOFT to verify the analytical results. The Parameter of linear model shown in Tab. 1 is used for computer simulation. By using the FEM simulation model with different operation parameters, characteristics of the magnetic flux shown in Fig.3 and Fig.4, the thrust, and the levitation force for the proposed NSLIM can be obtained.

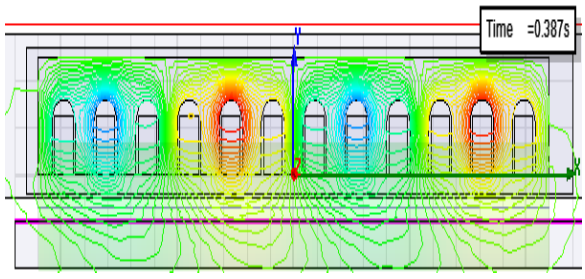

Fig. 3 flux density at ν = 0

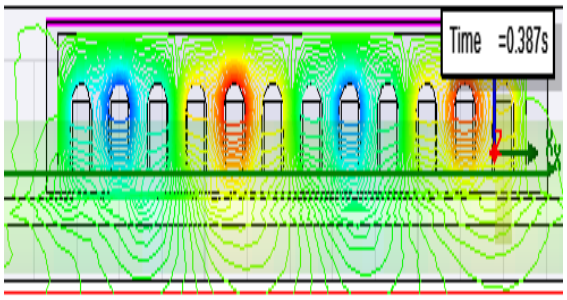

Fig. 4 Air-gap flux density at $v \neq 0$

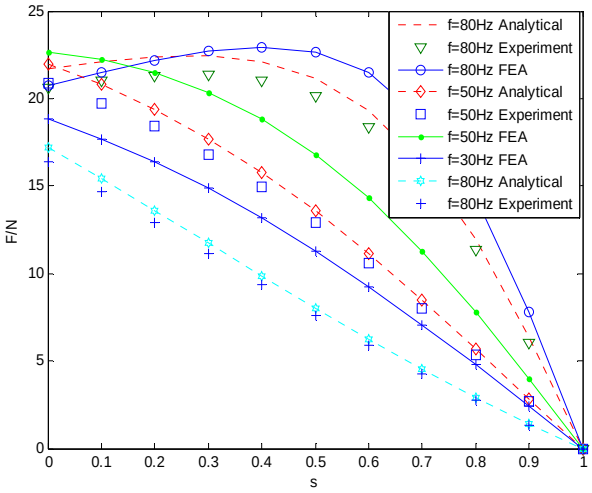

s -speed percent of synchronous speed;
Fig. 5 Thrust force curve under different frequency

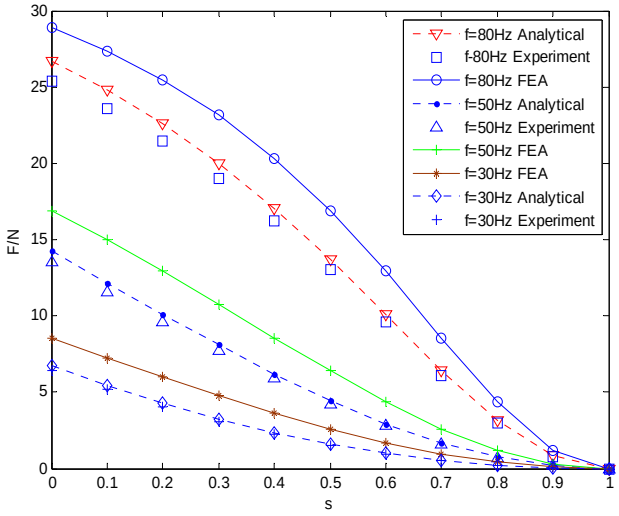

s -speed percent of synchronous speed;
Fig. 6 Levitation force curve under different frequency

Fig.5 and Fig.6 shows the slip-speed–force characteristics of the NSLIM with different input current frequencies. Curves in Fig. 5 show that the thrust increases as the input current frequency increases before the thrust is saturated. Curves in Fig.6 show that the lift increases as the input current frequency increases.

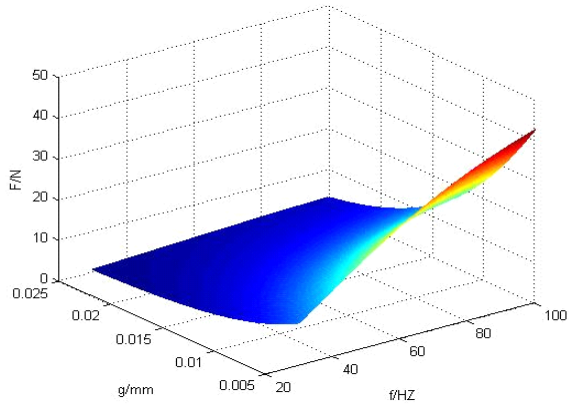

（a ）lift force

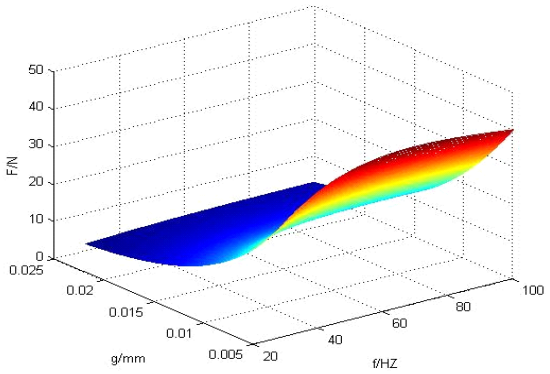

（b）thrust force
Fig.7 Force curve under different air-gap and frequency

Fig.7 shows the analytical results of the force characteristic for the NSLIM under different levitated heights with the different input current frequencies. For the linear region with the same slip speed, the curve indicates that the thrust increases as the input current frequencies decreases. Fig.7 (b) show that the lift increases as the air gap decreases and the input current frequencies increases.

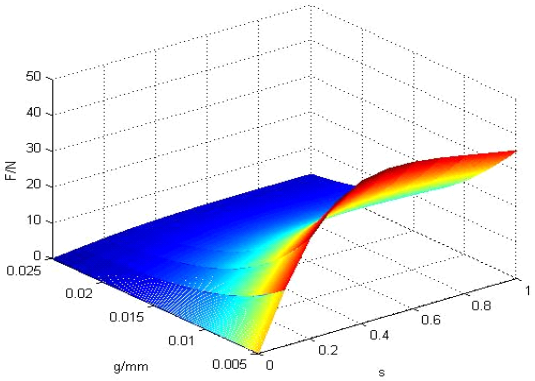

（a）thrust force

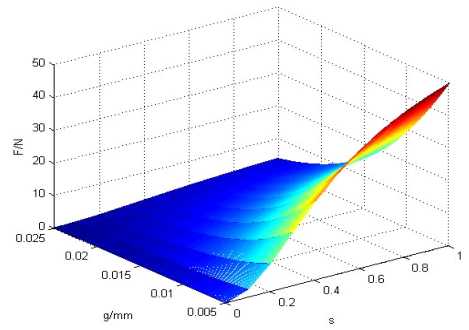

（b）lift force

Fig.8 Force curve under different air-gap and slip speed

Fig. 8 shows the analytical results of the force characteristic for the NSLIM under different the input current with the different slip-speed. Curve in Fig.8 (a) shows that the thrust increases as the air gap decreases and the larger slip-speed will produce a larger thrust before the thrust is saturated.

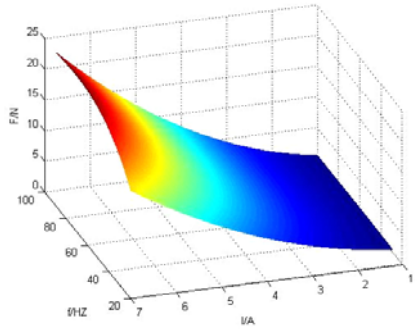

（a）Thrust force

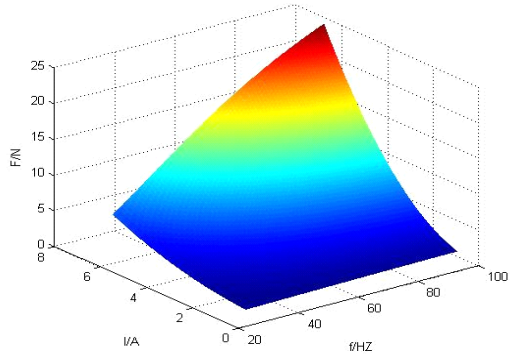

（b）lift force

Fig.9 Force curve under different phase current and frequency

Fig. 9 shows the analytical results of the force characteristic for the NSLIM under different the field current with the different input current frequencies. Curve in Fig.9 (a) shows that the thrust increases as the input current frequency increases and the larger current will produce a larger thrust before the thrust is saturated.

All in all, from the analytical-equation derivation and computer-simulation, it can be concluded that the NSLIM has similar characteristics of the induction motor [7].

4 CONCLUSIONS

This paper has presented the electromagnetic-force analysis for the NSLIM. The thrust and the levitation force of the proposed NSLIM can be achieved by using only a single power source. The analytical equations that reveal the relationship of the thrust and the levitation force with the mechanical structure of the proposed NSLIM are derived. The FEM computer simulations with different mechanical-structure parameters are performed to verify the analytical equations. The same trend can be found between the analytical equations and the computer-simulation results. Experimental measurements of the levitated heights of the rotor under different conditions are consistent with the expected trend given by the calculated and simulated results. The electromagnetic-force analysis performed in this paper can provide very useful information of mechanical-structure design and control-strategy development for the NSLIM.

REFERENCES

Lu Guang Yan., “Development and Application of the Maglev Transportation System,” I.E.E.E, Transactions on Applied Superconductivity, 18, 92, 2002.

Lu Guang Yan, “Suggestion for Selection of Maglev Option for Beijing-Shanghai High-Speed Line”, I.E.E.E, Transactions on Applied Superconductivity, 14, 936, 2004.

Wijono., H. Arof, H.W. Ping., “Analysis of magnetic field distribution of a cylindrical discrete Halbach permanent magnet linear generator,”, IET Electric Power Applications ,4, 629, 2010.

Yaow-Ming Chen, Shu-Yuan Fan and Wie-Shin Lu., “Electro-magnetic Force Analysis of the Magnetically Levitated Motor with Two Directions of Movement”, I.E.E.E, Transactions on Industry Applications, 42, 31, 2006.

LV Gang., SUN Shouguang., MA Yunshuang., “Efficiency optimal control of linear induction motor for urban rail transit.” , Electrical Machine and Control，13,490,2009.

LV Gang., FAN Yu, and MA Yunshuang, “Characteristic analysis of linear induction traction motor for urban rail transit.”, Electrical Machine and Control,14,77,2010,

Jonathan Bird, Thomas A. Lipo. , “Calculating the Force created by an Electro-dynamic Wheel Using a 2-D Steady-State Finite-Element Method,” I.E.E.E, Transactions on Magnetics ,44 , 365, 2008.